Roughness Change Effects for Small and Large Fetches

Sempreviva, A.M.; Larsen, Søren Ejling; Mortensen, Niels Gylling; Troen, Ib

Publication date:
1988

Document Version
Publisher's PDF, also known as Version of record

Risø-M-2749

RISØ

Risø-M-2749

Roughness Change Effects for Small and Large Fetches

Anna Maria Sempreviva, S.E. Larsen,
N.G. Mortensen, and I. Troen

Risø National Laboratory, DK-4000 Roskilde, Denmark
October 1988

Risø–M–2749

Roughness change effects for small and large fetches

Anna Maria Sempreviva, S.E. Larsen, N.G. Mortensen, and I. Troen

Abstract. Measurements were obtained during a two-year period along four meteorological masts placed from the coastline to 30 km inland at the North Sea coast of Jutland in Denmark (JYLEX).

From these data the near neutral cases were selected. The data are organized to show the reduction of wind speed as a function of inland fetch. The results are stratified according to season and are compared with a simple model description of the response of the neutral boundary layer to step changes in surface roughness.

Risø National Laboratory, DK-4000 Roskilde, Denmark

October 1988

ISBN-87–550–1467–4
ISSN 0418–6435

Grafisk Service, Risø, 1988

Contents

1 Introduction

When air under neutral conditions flows from one surface to another with a different roughness, an internal boundary layer (IBL) grows downwind from the roughness change. This phenomenon has been quite extensively described in literature for short fetches (e.g. Bradley (1968), Panofsky (1973), Businger (1972), Peterson et al. (1979), Rao et al. (1974)).

For long fetches the IBL grows until it fills up the planetary boundary layer and a new equilibrium is established between geostrophic wind and surface stress in accordance with the geostrophic drag laws. This part of the IBL growth has not been as thoroughly described as the short-fetch situation. Discussions are presented in Taylor (1969), Jensen (1978), Hedegaard and Larsen (1982) and Larsen et al. (1982).

In this paper we shall relate the problems of neutral flow response to changing roughness conditions to a data set obtained during the JYLEX experiment in which meteorological parameters were measured along four masts placed from the coastline to 30 km inland at the North Sea coast of Jutland in Denmark. The flow response will be discussed in terms of a close-to-neutral subset of these data and in terms of this data set combined with simple models describing the change of wind speed when moving inland from the sea.

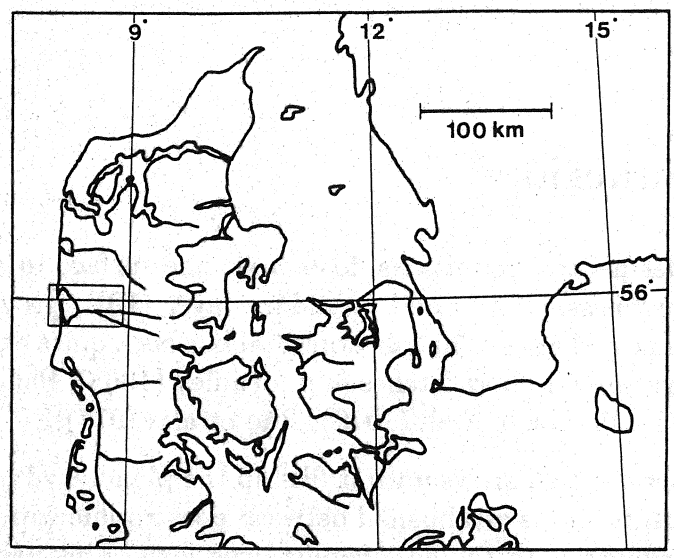

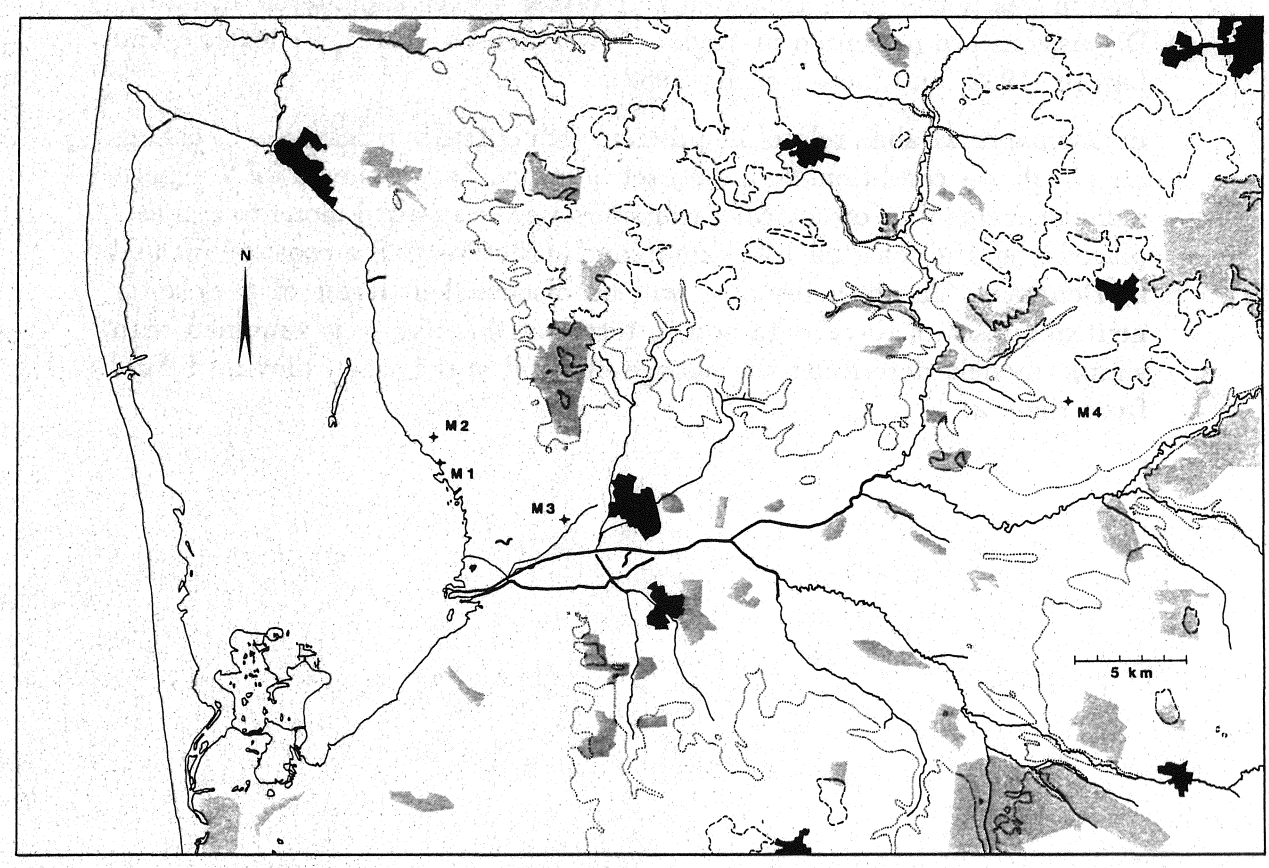

Figure 1: Maps of the experimental site. Figure 1a shows the overall area, while Fig. 1b gives a more detailed map of the site, indicating positions of the masts. In Fig. 1b main geographical features are also indicated such as cities (black areas), forests (shaded areas), and heights of terrain (20 and 50-m isolines). Positions of the measuring masts are indicated by M1, M2, M3, M4.

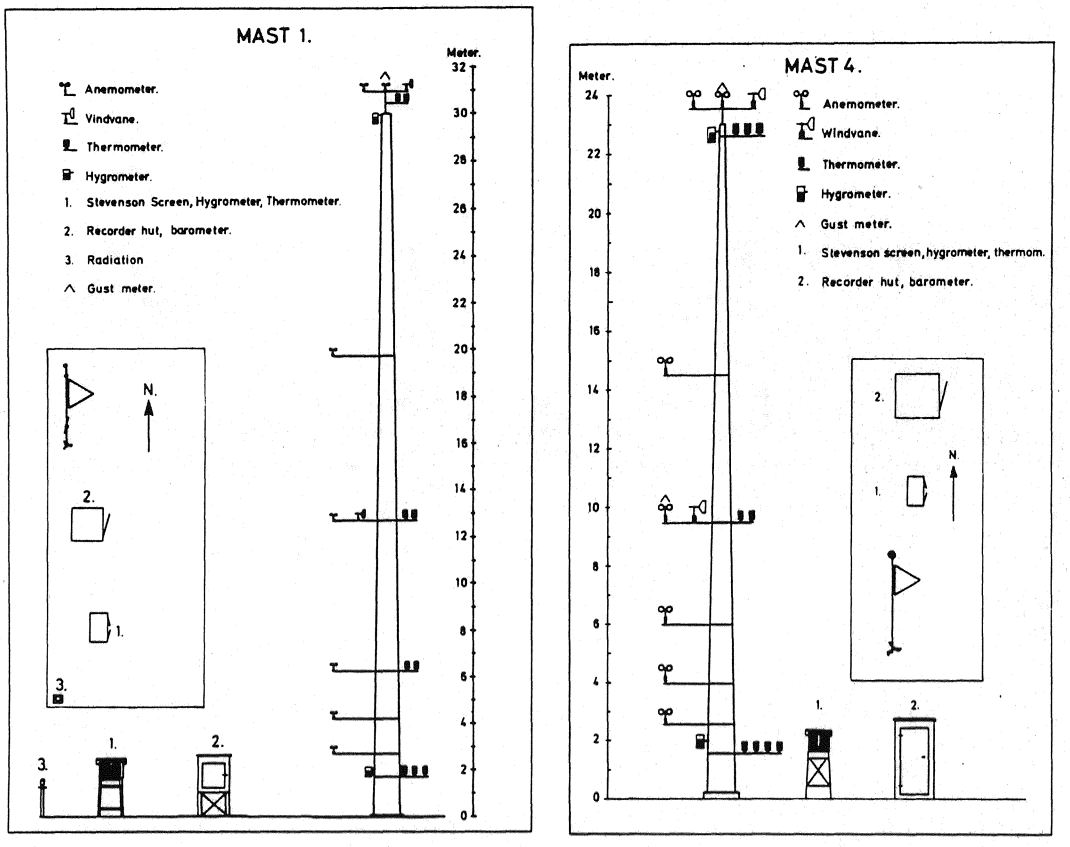

Figure 2: Appearance of the meteorological masts used during the experiment. Figure 2a shows the mast at the shore line, mast 1, while Fig. 2b shows one of the inland masts, mast 4.

2 The experimental set-up

The JYLEX experiment (JYLland EXperiment) was established on the west coast of Jylland (the Danish name for Jutland) to study the change of surface layer characteristics as a function of the distance from the sea.

Meteorological variables were measured along four masts placed from the shore line and up to 30 km inland. The positions of the masts are shown in Fig. 1. The shore-line mast M1 was a 32-m mast while the rest of the masts were 24 m high. Figure 2 illustrates the appearance of the shore-line mast and one of the inland masts. Table 1 summarizes the measurements conducted at each mast.

The experiment lasted from May 1982 until June 1984 yielding 25 months of data. The measurements were recorded every 10 minutes. Of the data used here wind speed was recorded as 10-min average values while wind direction and temperature were recorded as instantaneous values, although the response time of the instruments themselves provided some smoothing. The time constants of the wind vanes are about $20/u$ (u begin wind speed measured in m/s) while the thermometers had time constants of around 2 min; both values are from Mahrt and Larsen (1982) who used the same instrumentation.

In connection with change of recorder tapes (every three weeks), photographs were taken of the surroundings of each mast to record the seasonal variation of the vegetation.

The experiment was originally conceived as a straight line of masts reaching from the west coast of Jutland towards the east. It appears from Fig. 1 that the final set-up neither started at the shore line of the North Sea nor can be described a straight line. Avoiding flow-obstructing features in the near field around each mast had the highest priority, and the final set-up was a result of this. Even in this fairly flat part of Denmark, such features were abundant either in the form of coastal brinks, dunes and dikes at the coast or hills, houses and trees further inland.

Table 1: The JYLEX experiment. For each of the four masts are shown distance to the coast, height, and number of measurement levels for the various parameters.

Station	Mast 1	Mast 2	Mast 3	Mast 4
Distance to coast [km]	0.08	1.2	4.4	30.2
Height of mast [m]	32	24	24	24
Wind speed	6	3	3	6
Wind direction	2	2	2	2
Gust wind speed	1	1	1	1
Temperature	2	2	2	2
Temperature gradient	4	2	2	4
Relative humidity	3	1	1	3
Precipitation			1	
Atmospheric pressure	1			1
Incoming short-wave	1		1	
Sonic anemometer			1	

3 Data selection and analysis

The present study is concerned with the change of wind speed as the air moves inland from the sea under near-neutral conditions. Therefore, a subset of data was selected according to the following criteria:

a) Data were to be included only if the wind came from a 90° westerly sector at mast 1.

b) Data should be available at all four masts.

c) Near-neutral data were ensured by demanding a wind speed larger than 12 m/s at the top level of mast 1 while at the same time the absolute value of the Richardson number should be less than 0.03 at all masts. The Richardson number used refers to 10-m height.

The data set selected in this way consisted of 2048 sets of profile data recorded simultaneously along each mast, meaning that 2 per cent of the data fulfilled the above criteria. It was stratified subsequently according to the following criteria.

1. Day or night

2. Season: winter (December, January, and February
   spring (March, April, and May)
   summer (June, July, and August)
   fall (September, October, and November).

3. Finally, the 90° direction sector was subdivided into nine 10° sectors.

The day/night and seasonal criteria both stratified the data according to thermal effects that might prevail, in spite of the effort to ensure neutral conditions. Larsen and Jensen (1983) found that, for the Danish climate, the temperature of the water surface is 1° C colder than the daily average temperature of the air over land during spring and 1° C warmer in fall. However, the most important reason for introducing the seasonal criterion is that the roughness over land varies with season following the vegetation and other aspects of the surface such as snow cover and tilling of the farmland.

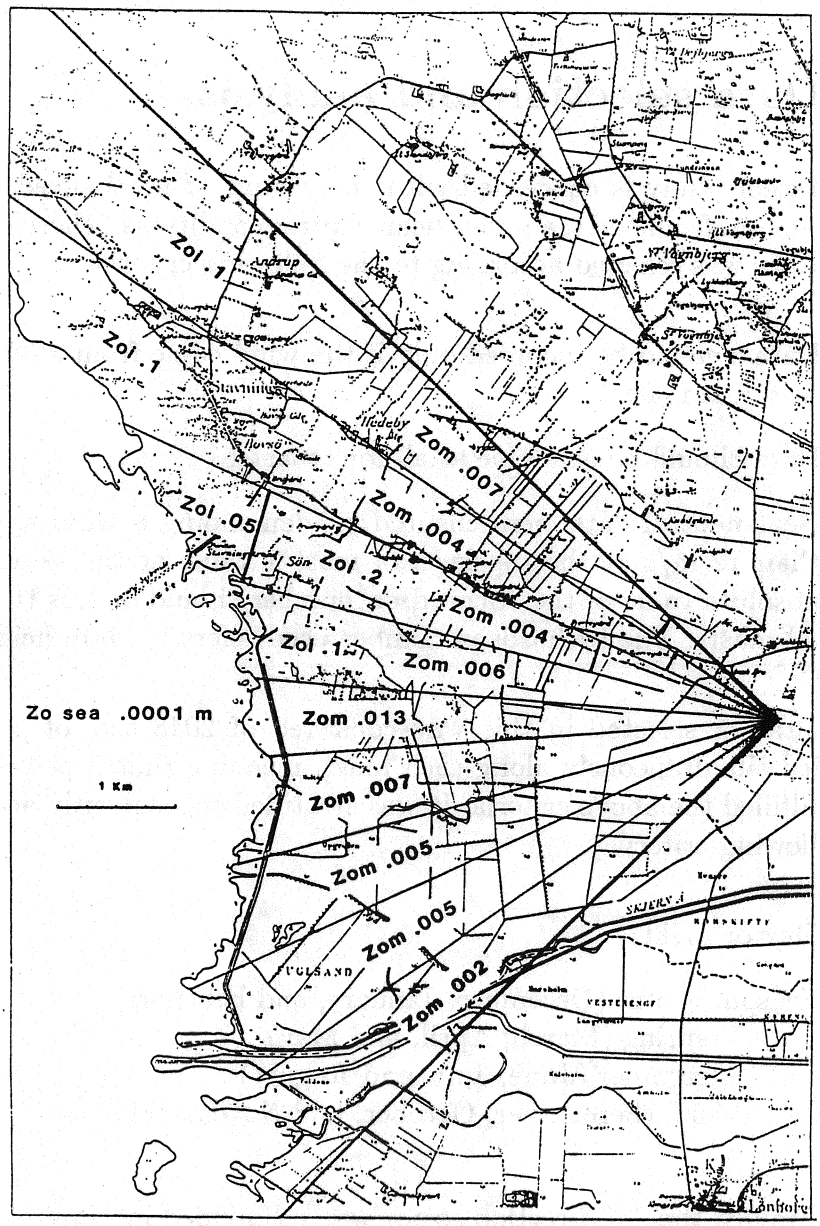

Figure 3: Layout of the nine westerly direction sectors from each mast, here mast 3. Also shown in the figure is how different roughness values are ascribed to different areas for use in the model computations. z_{0m}-values are estimated from the profile measurements, while the z_{0i}-values are estimated as described in the text. Many of the z_{0i}-areas in the figure are further subdivided into areas with different z_{0i}. For simplicity this is omitted in the figure.

The subdivision into 10° direction sectors was made because it allowed us to determine fairly well-defined fetch conditions for each mast. The appropriate wind direction sectors were determined on the basis of the measurements at mast 1. However, during the strong wind conditions considered here it was found that all masts always showed a wind direction within the same 10° sector. Figure 3 illustrates the direction sectors for mast 3.

Between the velocity u_i at mast i (i = 2,3,4) and the upstream over-water velocity u_1 the ratios were calculated for each record at the 24-m level. Subsequently, the average values and standard deviations of these ratios were computed within each bin defined by the day/night, season and wind direction criteria given above.

As said above, the upstream wind was determined from mast 1. Due to the presence of an approximately 100-m wide rush field in front of mast 1, we used the 31-m wind (see Fig. 2) to estimate the over-water wind at the height of 24 m. This was done using Charnock's relation in conjunction with a logarithmic wind profile.

$$\begin{aligned} u_* &= \kappa\, u_{31}/\ln(31/z_{0w}) \\ z_{0w} &= c\, u_*^2/g \\ u_{24} &= \frac{u_*}{\kappa}\ln(24/z_{0w}) \text{ with } c = (1.4 \times 10^{-2}) \end{aligned} \tag{1}$$

where z_{0w} is the water roughness length. Initial computations of the average velocity ratios within bins showed no significant difference between night and day bins, lending some credibility to our neglect of thermal effects. In the discussion below we shall therefore consider only data stratified according to season and sectors. Within these bins the total amount of 10-min averaged data is summarized in Table 2.

The distance to the water from each mast is summarized for each sector in Appendix A. Having determined these distances, the sector and seasonal averages of u_i/u_1, the corresponding standard deviations can be plotted versus land fetch. This is done in Fig. 4 for the winter and summer data.

The velocity ratio is generally seen to decrease with increasing fetches. However, there is considerable scatter. This reflects that plotting $\langle u_i/u_1 \rangle$ versus fetch only is a strong idealization. In reality, the velocity at each mast reflects the upstream history of the flow, and with few exceptions a

Table 2: Number of 10-min records used for estimating the sector and seasonal average of u_i/u_1, in which the subscript refers to the mast number.

Direction	Sector	Season				Year
		Winter	Spring	Summer	Fall	
230°	1	51	37	13	29	130
240°	2	53	13	15	38	119
250°	3	163	7	27	83	280
260°	4	149	24	12	46	231
270°	5	132	24	51	37	244
280°	6	98	20	50	41	209
290°	7	122	51	35	41	249
300°	8	55	62	113	47	277
310°	9	12	46	189	62	309
225°-315°		835	284	505	424	2048

trajectory passing one mast will not pass any of the others. However, in the following we shall use the idealized picture at least to the extent that we will use the velocity at mast 1 as upstream over-water conditions for all masts.

Figure 4 shows also that the standard deviation of each $\langle u_i/u_1 \rangle$ increases with increasing fetch. This can simply be explained by noting that the correlation between u_1 and u_i fluctuations is getting smaller for the larger distances involved in spite of the 10-min averaging employed.

In Fig. 5 this point is elaborated. Here, we show for each mast the difference between the value of $\langle u_i/u_1 \rangle$ averaged over sector 2 through 8 and the corresponding annual average i.e., for each mast we take the difference between

$$\begin{aligned} \langle \frac{u_i}{u_1} \rangle_{season} &= \frac{1}{7} \sum_{sector 2-8} \langle \frac{u_i}{u_1} \rangle_{season,sector} \\ \langle \frac{u_i}{u_1} \rangle_{year} &= \frac{1}{4} \sum_{season} \langle \frac{u_i}{u_1} \rangle_{season} \end{aligned} \tag{2}$$

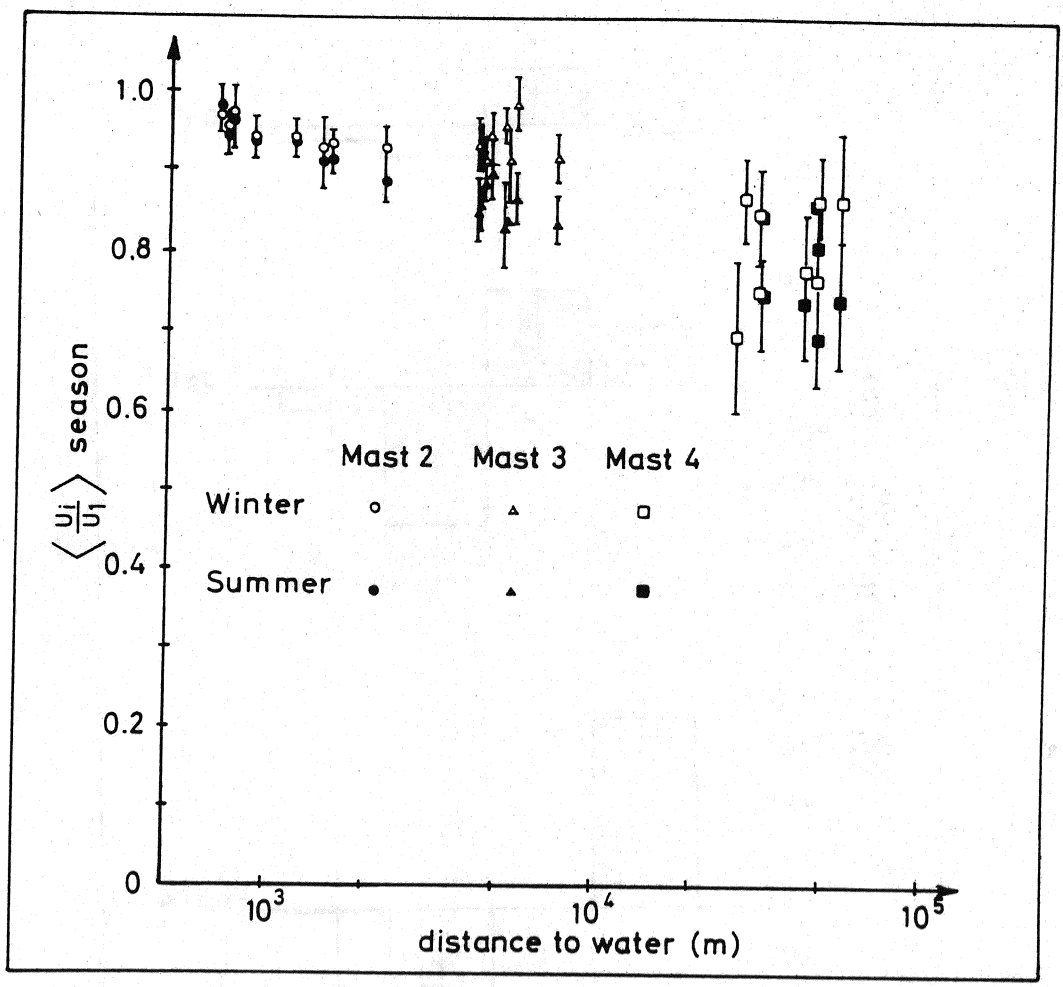

Figure 4: The figure shows $\langle u_i/u_1 \rangle$, i = 2,3,4 where u_i is the velocity at a height of 24 m at mast i and the averaging pertains to sectors and seasons. The ratio is plotted versus distance to the water (see Appendix A) for each mast. Only the ratios for winter and summer seasons are shown. The bars indicate the standard deviation on the estimated $\langle u_i/u_1 \rangle$. The figure shows that the winter data seem to lie above the summer data, reflecting, we believe, a generally higher land roughness during the summer.

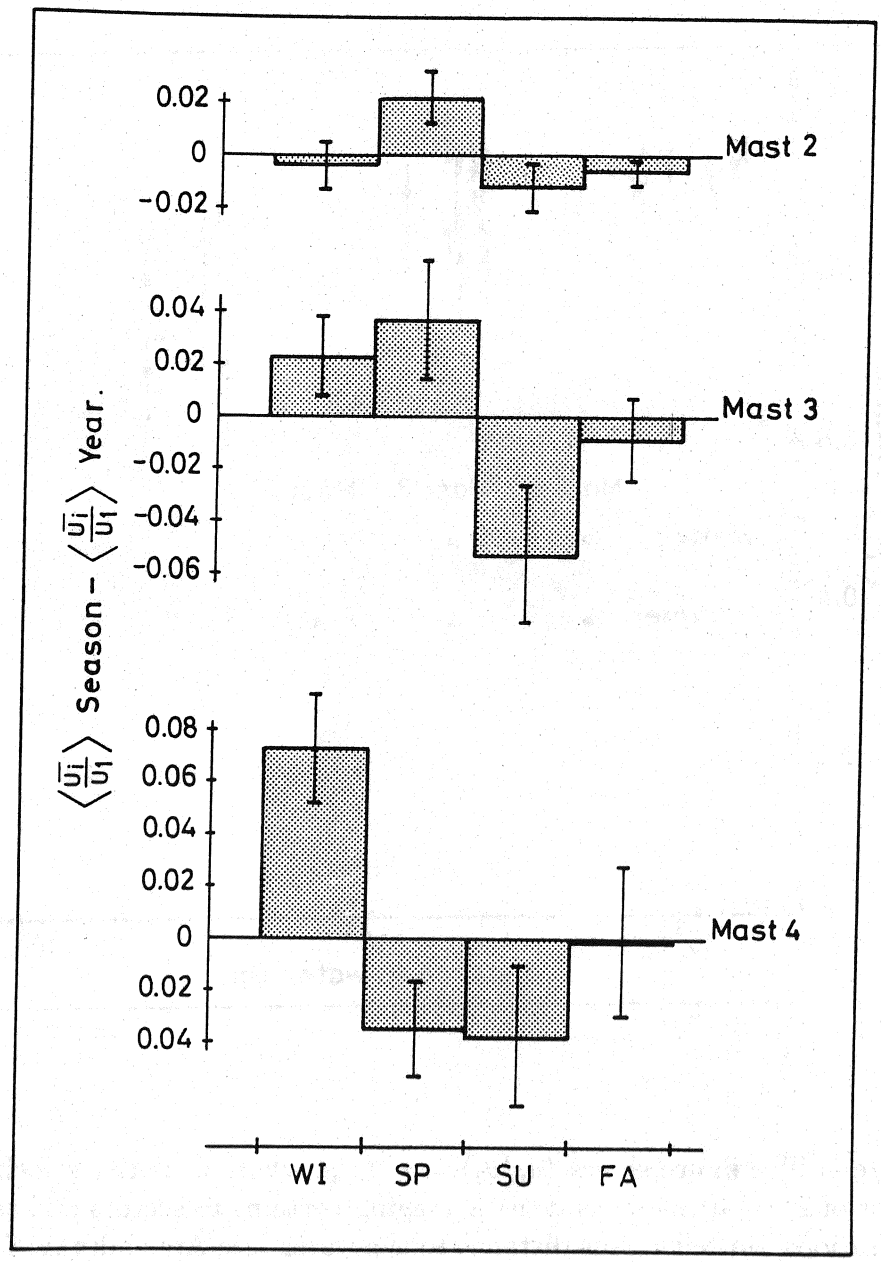

Figure 5: Seasonal variation of $\langle u_i/u_1 \rangle$ averaged over sectors 2–8 (see (2)) for the different masts. The bars indicate standard deviation on sector average shown by overbar of $\langle u_i/u_1 \rangle$.

As already indicated in Fig. 4, winter data are generally high and summer data low while the spring and fall data are less clear. As mentioned above, this behaviour probably reflects a mostly vegetation-controlled variation of the land roughness. As a detail, we note that the winter value is below average for mast 2. This undoubtedly reflects the cycle of growing and harvesting of the 100-m rush zone in front of mast 1. This zone is harvested at the end of February and in the beginning of March. The rush grows to a height of about 2 m in late summer and remains at this height during winter. It is likely that this rush zone does not influence the 31-m velocity at mast 1 (at least not for sectors 2–8), but it certainly influences the velocity at mast 2, being 1 km downwind from this zone.

4 Model description

For comparison with the data, we present here a simple model for describing the flow response to step changes in surface roughness.

The first part of the model is described in Hedegaard and Larsen (1982) and Larsen et al. (1982); originally, this model comes from Miyake (1965) and is further discussed in Panofsky (1973), Businger (1972) and Jensen (1978)).

When the flow passes a change in surface roughness, an internal boundary layer grows as

$$\frac{\partial h}{\partial x} = A \cdot \frac{\sigma_w(h)}{u(h)} \tag{3}$$

in which h is the height of the internal boundary layer, x is the fetch downwind of the roughness change, while u is the mean speed and σ_w the standard deviation of the vertical wind speed. The two last parameters are described by

$$\begin{aligned} u &= \frac{u_{*0}}{\kappa}\left(\ln\frac{z}{z_0} - 2\frac{z}{H}\right) \\ \sigma_w/u_{*0} &= \frac{\sigma_{w0}}{u_{*0}}\left(1-\frac{z}{H}\right)^2 \\ H &= u_{*0}/f \end{aligned} \tag{4}$$

in which f is the Coriolis parameter, κ the von Kármán constant, z_0 the roughness length, and H the scale height. Subscript 0 indicates that the parameter refers to the surface.

Integration of Eqs. (3) and (4) yields

$$c\frac{x}{z_0} - 1 = \frac{\frac{h}{z_0}}{1-\frac{h}{H}}\left(\left(\ln\frac{h}{z_0} - 1\right) - y\left(\frac{h}{H}\right)\right) \tag{5}$$

with $y\left(\frac{h}{H}\right) \sim \frac{h}{H}$ and c is a coefficient of the order one.

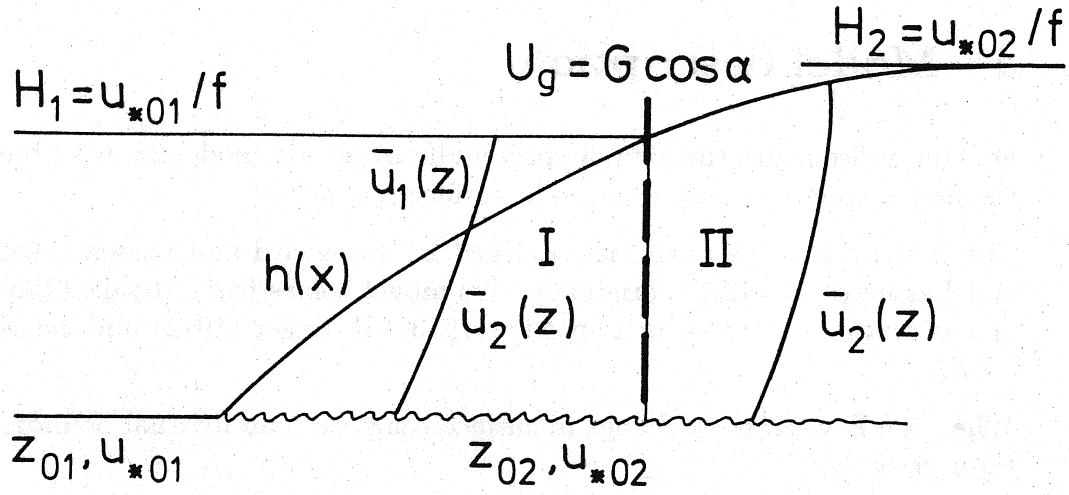

Figure 6: Growth of an internal boundary layer (IBL) in a two-dimensional planetary boundary layer (PBL) for smooth-to-rough transition. In Zone I the IBL grows within the smooth PBL, while in Zone II $h(x)$ is above the smooth PBL (Larsen et al., 1982).

For $z/H << 1$, the expression for u in Eq.(4) has the usual logarithmic form and reduces to a one-dimensional drag law as $z \rightarrow H$. From Tennekes (1973) the neutral drag law can be written

$$\begin{aligned} U_G &= \frac{u_{*0}}{\kappa}\left(ln\frac{H}{z_0} - 2\right) \\ V_G &= -12u_{*0} \\ G^2 &= U_G^2 + V_G^2 \end{aligned} \tag{6}$$

where G is the geostrophic wind and U_G, V_G its components in a coordinate system aligned with the surface wind.

A transition from a smooth to a rough surface is depicted in Fig. 6. By matching the upstream wind profile $u_1(z)$ and the downwind profile $u_2(z)$ at $h(x)$, we obtain for $h \leq H_1$ (Zone I in Fig. 6)

$$\frac{u_{*02}}{u_{*01}} = \frac{\ln \frac{h}{z_{01}} - 2\frac{h}{H_1}}{\ln \frac{h}{z_{02}} - 2\frac{h}{H_2}} \tag{7}$$

and for $h \geq H_2$ (Zone II in Fig. 6)

$$\frac{u_{*02}}{u_{*01}} = \frac{\ln \frac{H_1}{z_{01}} - 2}{\ln \frac{h}{z_{02}} - 2\frac{h}{H_2}} \tag{8}$$

in which it is assumed that both profiles are described by equilibrium expressions as Eq. (4).

Assuming $\frac{h}{H} \rightarrow 0$ in the above equations, we recover the surface layer expressions suggested by Miyake (1965), corresponding to Eqs. (4) and (7)

$$\begin{aligned} c\frac{x}{z_0} - 1 &= \frac{h}{z_0}\left(\ln \frac{h}{z_0} - 1\right) \\ \frac{u_{*02}}{u_{*01}} &= \frac{ln\frac{h}{z_{01}}}{\ln \frac{h}{z_{02}}} \end{aligned} \tag{9}$$

The coefficient c in Eqs. (5) and (9) can be calibrated by comparison with measured stress ratios. This yields $c \sim 1$. Here, we follow Larsen et al. (1982) in using $c = 0.9$.

As the IBL grows, the surface wind must turn to approach the drag law, Eq. (6), for the new equilibrium boundary layer. In Larsen et al. (1982) this is suggested to be taken into account by

$$\sin \alpha = \frac{V_G}{G} = \begin{cases} -12H_1 f/G & \text{for} \quad h \leq H_1 \\ -12hf/G & \text{for} \quad H_1 < h \leq H_2 \end{cases} \tag{10}$$

With this approach the surface stress ratio in Eq. (8) is modified to

$$\frac{u_{*02}}{u_{*01}} = \frac{\cos \alpha}{\cos \alpha_1} \frac{\left(\ln \frac{H_1}{z_{01}} - 2\right)}{\left(\ln \frac{h}{z_{02}} - 2\frac{h}{H}\right)} \tag{11}$$

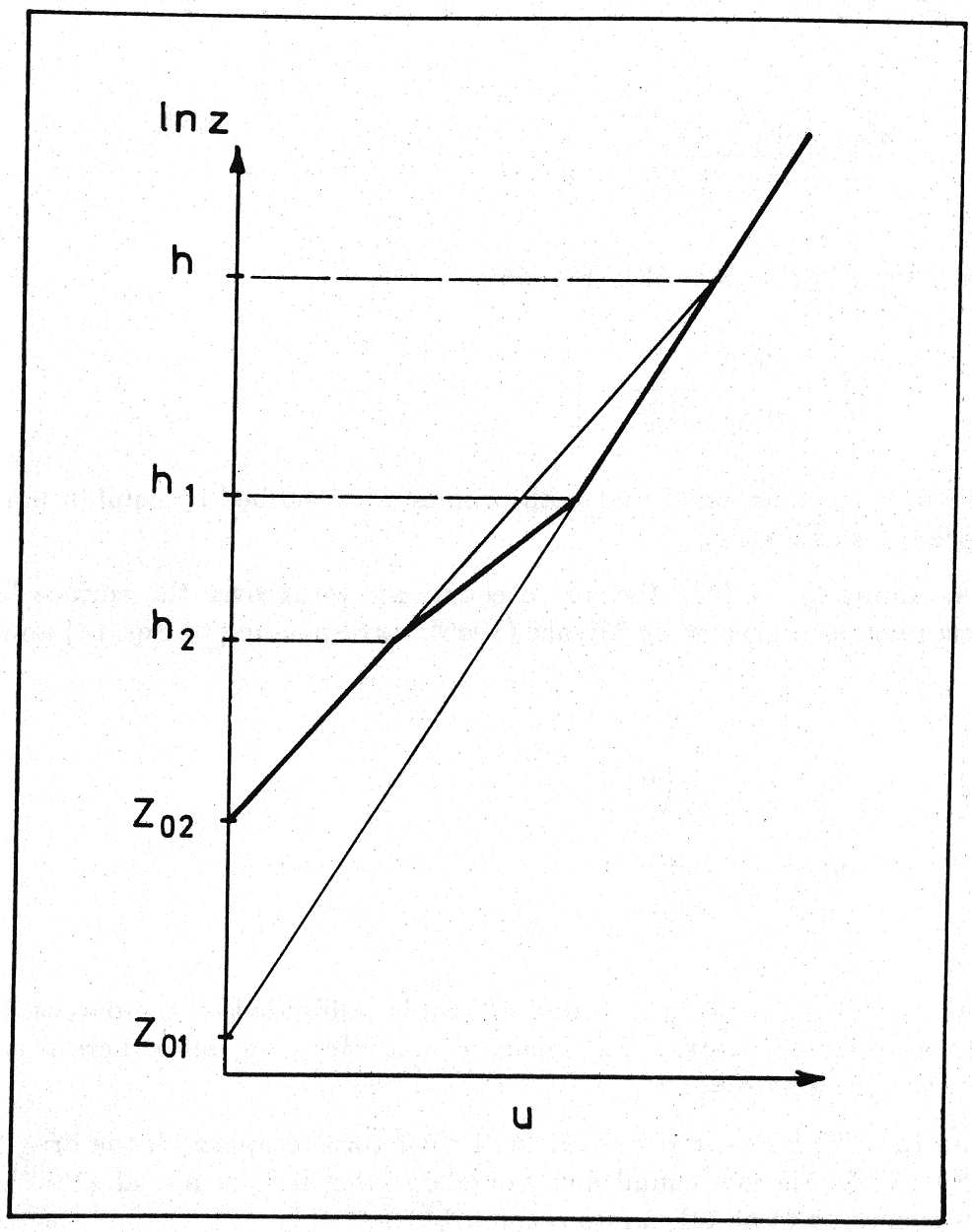

Figure 7: Behaviour of the velocity profile in an internal boundary layer for a smooth-to-rough-transition according to Jensen (1977). The outer and inner profiles (thin lines) are matched at $z = h$. The profile in equilibrium with the surface stress of the IBL reaches up to $z = h_2$ ($\sim$ between $\frac{1}{10}$ and $\frac{1}{20}$ of h). The outer profile reaches down to $h_1 \sim \frac{1}{3}h$. For $h_2 < h < h_1$ the profile is interpolated. For rough-to-smooth transition the kink reverses.

where α_1 is the α pertaining to area one.

So far the discussions have been concerned with the smooth to rough transition. This transition is characterised by a more turbulent IBL growing through a less turbulent planetary boundary layer. The rough to smooth transition, on the other hand, is characterised by a dying of the turbulence in the more turbulent PBL to make room for the growth of the less turbulent IBL. Hence, the physics is quite different. However, it is found that the surface layer model, Eq. (9), describes both types of transitions quite well provided that the z_0-value used in the equation for $h(x)$ is the one pertaining to the rougher surface (Panofsky (1973), Jensen (1978)). Larsen et al. (1982) suggest use of the same rule for the extended model in Eq. (5) in which both z_0 and H now must pertain to the rougher surface and to stop the growth of h when reaching the scale height H_2, that for the rough to smooth transition is smaller than H_1.

As formulated above, the model predicts the stress ratio for upstream and downstream conditions. To predict the corresponding wind speed ratios the equilibrium profiles are used, yielding a wind speed ratio as

$$\frac{u_2(z)}{u_1(z)} = \frac{u_{*02}}{u_{*01}} \frac{\ln \frac{z}{z_{02}} - 2\frac{z}{H_2}}{\ln \frac{z}{z_{01}} - 2\frac{z}{H_1}} \quad , \tag{12}$$

where the u_*-ratio is given by Eqs. (7) and (11).

However, we shall employ here an idea by Jensen (1977). From comparison with experimental data and numerical models by Peterson (1972), Taylor (1969) and Rao et al. (1974), he concluded that the profiles could be best described by the model shown in Fig. 7 for the smooth-to-rough transition. Here, the u_* ratio is still found by matching the equilibrium profiles at $z = h(x)$. However, the outer profile is found to extend down to $z = h_1 \sim \frac{1}{3}h(x)$, while the inner profile, being in equilibrium with u_{*02}, extends up to $z = h_2 \sim 0.1h(x)$. Between h_1 and h_2 we shall simply interpolate linearly, i.e.

$$u(z) = u(h_2) + (u(h_1) - u(h_2))\frac{\ln z - \ln h_2}{\ln h_1 - \ln h_2} \quad . \tag{13}$$

For use in situations with several roughness changes the above model formulations are applied as follows (Larsen et al., 1982, Petersen and Troen, 1986)

$$u_n/u_0 = \Pi_{i=0}^{n-1} u_{i+1}(x_{i+1})/u_i(x_i) \quad , \tag{14}$$

in which x_i is the distance between the point where u_n is estimated and the location of roughness change n_i, considering u_0 as an equilibrium upstream condition.

In the next sections we shall compare the JYLEX data with aspects of the above model construction. Therefore, it seems reasonable with a short discussion of what is known about its validity.

For short fetches, say $x < 100$ m, the surface layer description in Eq. (9) is known to be the most successful of all models available in describing the surface stress ratio (Jensen, 1978).

The extended model Eq. (5) through Eq. (12) could be superior to the surface layer model for slightly larger fetches as long as growth of the IBL remains controlled by diffusion, because it allows for a decrease of the turbulence level with height. Furthermore, it has the advantage that the stress ratio formally approaches the value found between the two equilibrium boundary layers as the fetch goes to infinity. However, it does not contain any of the physics involved when the fetches approach the Ekman length G/f for which pressure and Coriolis forces will be responsible for the final approach to equilibrium. The model was tested by Hedegaard and Larsen (1982) and Larsen et al. (1982) on climatological data, and it was concluded that the model tended to approach equilibrium too slowly, but that it worked reasonably well out to fetches of the order of 30–40 km. However, the comparison with data was made uncertain by the uncertainty of estimating the surface roughness for extended areas, a problem we will have to face also in the present paper. As far as we know, the shape of the profile shown in Fig. 7 has not been much used in connection with the type of model described here. However, the different numerical models with second-order turbulence closure are all quite consistent in predicting this kind of shape.

5 Determination of the surface roughness

To compare the model prediction with measurements, the roughness of the environment must be determined for each mast in each of the nine sectors considered. This involves for each sector and mast a determination of the distance from the mast to each roughness change as well as the values of relevant roughness lengths. The method is illustrated in Fig. 3, and details of the roughness determination are described in Appendix A in which are also shown the actual values used.

The fetches to each roughness change were determined from maps as well as from inspection of the area. Here, the first change in front of a mast was best defined because a mast was typically placed on the eastern side of a field to obtain a maximum homogeneous and unobstructed fetch for westerly flows. The roughness of this near field was also quite well determined, since it was found from velocity profiles of the data set to be compared with model predictions.

As regards the areas further away from the masts, both fetches and roughness values became less well defined. We used the methods recommended in Jensen et al. (1984) and Petersen and Troen (1986). The actual roughness values were estimated from Table A5.

The roughness values thus determined deviate in several ways from the near-field roughness. Since the near-field roughnesses are measured data, they follow the cycles of vegetation and tilling for each particular site. Hence, different z_0-values are used in different seasons (see tables in Appendix A). This is not so for the large-scale roughness values as deduced from Table A5. They generally pertain to types of terrain with a mixed combination of roughness elements, i.e. fields, houses, trees and hedges. How the roughness of such areas will vary with season, if at all, is not well-known. Later on we shall revert to the problem of comparison between data and model. Furthermore, the estimated roughness value does not exhibit a clear seasonal variation, and the annual mean values are associated with fairly large uncertainties (of the order of ± 20 per cent as is obvious from Table A5.

Also the upstream water roughness should be discussed. As argued in connection with Eq. (1) we use Charnock's relation where the coefficient cited, $c \sim 1.4 \times 10^{-2}$ is estimated mostly from data pertaining to the open ocean, which obviously are different from the present upstream conditions needed here. Therefore, we have tested the model performance for various values of c, as will be discussed below.

6 Comparison between model and data

The models described in Section 4 have been used to compute u_i/u_1 for $z = 24$ m for each sector, mast and season. The computed u_i/u_1 are compared with the corresponding $\langle u_i/u_1 \rangle$ values obtained from the data set as discussed in the first sections of this paper.

For the detailed comparison, we define the relative deviation as

$$\delta = 100 \cdot \left(\langle \frac{u_i}{u_1} \rangle_{exp} - \left(\frac{u_i}{u_1} \right)_{comp} \right) / \langle \frac{u_i}{u_1} \rangle_{exp} \tag{15}$$

where δ now is defined for each of the masts 2, 3 and 4, sector and season.

As discussed in the preceding section, the estimate of the surrounding roughness at each mast is associated with quite some uncertainty. Therefore, we cannot test in a strict sense the absolute validity of the model approaches considered. Instead we will address the following uncertainties:

a) How will δ change with a changing estimate of the water roughness?

b) What is the influence on δ when using the extended BL model rather than the surface layer model given by Eq. (9)?

c) How does introduction of the kinked profile in Fig. 7 influence δ?

As a basic model we choose the extended BL model given by Eqs. (5) and (6). The kinked profile is used with $h_1 = h/3$ and $h_2 = h/15$. The upstream water roughness is determined by Charnock's constant $c \sim 1.4 \times 10^{-2}$. Tables 3, 4 and 5 illustrate how δ changes when we change one of the aspects considered under questions a) to c) in turn, keeping the other model characteristics as in the basic model.

For evaluation of the results in the tables we average δ over sectors 2–8 for each mast and season. (For reasons discussed in Appendix A we do not include sectors 1 and 9 in the averaging as these sectors were neglected also in the compilation of Fig. 5). The averaged δ is denoted $\bar{\delta}$.

Table 3: The effect on δ [%] in Eq. (15) of changing Charnock's constant in the formula for the upstream water roughness. $\bar{\delta}$ is the average of δ over sectors 2–8, σ is the corresponding standard deviation.

Season	$\bar{\delta}M_2$	σM_2	$\bar{\delta}M_3$	σM_3	$\bar{\delta}M_4$	σM_4	c
winter	0.9	1.2	3.1	2.0	12.8	2.8	5×10^{-3}
spring	2.2	1.1	5.8	2.7	0.8	2.8	
summer	2.0	1.6	4.1	4.0	–2.3	5.7	
fall	2.1	1.3	3.7	2.5	5.1	2.4	
year	1.8		4.2		5.3		
winter	–0.2	0.9	0.7	2.0	10.0	2.9	1.4×10^{-2}
spring	1.4	1.1	3.7	2.9	–2.2	2.8	
summer	1.1	1.5	2.1	4.0	–1.0	5.3	
fall	1.1	1.0	1.5	2.5	2.2	2.5	
year	0.9		2.0		2.3		
winter	–1.7	0.7	–2.6	1.9	6.0	3.0	4.2×10^{-2}
spring	0.2	1.5	0.7	3.11	–6.4	2.9	
summer	–0.1	1.5	–0.8	4.0	–4.9	5.5	
fall	–0.3	1.0	1.6	1.7	–1.9	4.3	
year	–0.5		–1.1		–1.8		

First, we study the influence of changing Charnock's constant. The results are summarized in Table 3. The c-value producing $\bar{\delta}$ close to zero for all three masts is seen to be between 1.4×10^{-2} and 4.2×10^{-2} around $c \sim 3.0 \times 10^{-2}$. This value is somewhat larger than the "normal" value 1.4×10^{-2}. However, the nearest part of the upstream conditions is either the shallow fjord or the coastal water (see Fig. 1). It is therefore not surprising to find z_0 somewhat larger than the "open-ocean" value (see e.g. Geernaert et al., 1987). The value of z_0 found here corresponds closely to the drag coefficient values reported by Geernaert et al. from measurements in the North Sea. It should be pointed out that changing c does change the extrapolated u_1 (24 m) as seen from Eq. (1). This equation shows, however, that these changes are quite negligible.

Table 4: The effect on $\bar{\delta}$ [%] (Eq. (15)) of changing the value of h_1, (Fig. 7). $\bar{\delta}$ is the average of δ over sectors 2–8, and σ is the corresponding standard deviation.

Season	$\bar{\delta}M_2$	σM_2	δM_3	σM_3	δM_4	σM_4	h_1
winter	–0.2	0.9	0.7	2.0	10.0	2.9	$\frac{1}{3}h$
spring	1.4	1.1	3.1	2.9	–2.2	2.8	
summer	1.1	1.5	2.1	4.0	–1.0	5.3	
fall	1.1	1.0	1.5	2.5	2.2	2.4	
year	0.9		2.0		2.3		
winter	–0.0	0.6	0.2	1.5	7.4	2.9	$\frac{1}{2}h$
spring	2.2	1.5	3.2	3.2	–5.1	2.7	
summer	2.9	1.5	1.9	3.9	–3.5	5.3	
fall	2.1	0.8	1.1	2.2	–0.2	3.4	
year	1.8		1.6		–0.3		
winter	0.3	0.8	–0.2	1.3	4.9	3.0	h
spring	3.1	2.1	2.8	3.6	–8.0	2.7	
summer	4.8	2.0	1.7	3.9	–5.8	5.2	
fall	3.1	1.2	0.8	2.1	–2.6	4.1	
year	2.8		1.2		–2.9		

Next we shall study the influence on δ of changing the height, h_1, down to which the outer profile is supposed to describe the resulting profile (see Fig. 7). Here, our basic situation is $h_1 \sim h/3$, and we shall see the effect of increasing this height to $h/2$ and h, where the last value corresponds to the velocity profile being found just by matching the inner and outer profile in $z = h$. The results are shown in Table 4 and as can be seen, tendencies are different at the different masts. The reason is that the response to changing h_1 will depend on the number and character of the roughness changes experienced by the flow on its way to the measuring mast, as well as of the measuring height.

Finally, we study the importance of the model behaviour for large fetches. Table 5 shows the result. The first case is our basic model, next is the surface layer model described by Eq. (9) while in the last case we study

Table 5: The effect on δ [%] (Eq. (15)) of changing model behaviour for large fetches.

Season	$\bar{\delta}M_2$	σM_2	$\bar{\delta}M_3$	σM_3	$\bar{\delta}M_4$	σM_4	IBL growth
winter	–0.2	0.9	0.7	2.0	10.0	2.9	$h \to H$
spring	1.4	1.1	3.1	2.9	–2.2	2.8	as
summer	1.1	1.5	2.1	4.0	1.0	5.3	$x \to \infty$
fall	1.1	1.0	1.5	2.5	2.2	2.4	
year	0.9		2.0		2.3		
winter	–0.2	0.9	0.8	2.0	11.4	3.0	
spring	1.5	1.1	3.8	2.9	–0.3	2.9	$h \to \infty$
summer	1.3	1.5	2.5	4.0	1.2	5.3	as
fall	1.2	1.0	1.7	2.5	4.0	2.7	$x \to \infty$
year	1.0		2.2		4.1		
winter	–0.2	0.9	0.7	2.0	14.2	3.0	
spring	1.5	1.1	3.1	2.9	2.4	3.4	$h = H$
summer	1.3	1.5	2.1	4.0	3.3	6.2	$x \geq 10$ km
fall	1.2	1.0	1.5	2.5	6.6	4.4	
year	1.0		2.0		6.6		

the effect of forcing the internal boundary to equilibrium of a 10-km fetch. The reason for this is that the two former models are unrealistic for large fetches. The surface layer model does not approach a new equilibrium at all, while this is the case for the extended model, however, the necessary fetches are so long fetches that it seems unrealistic.

The uppermost results in Table 5 pertain to the standard model, Eq. (5), the results in the middle refer to the surface layer model, Eq. (9). The last example is like our basic model for $x < 10$ km. For $x \geq 10$ km, h is then forced to $H = u_*/f$. It appears from the table that the extended model fares best, however, only marginally better than the pure surface layer model. Given the uncertainty of the large-scale and upstream-water roughnesses, it is better to say that the two models perform equally well.

The last case, in which the IBL is forced to equilibrium by forcing $h \rightarrow H$ when $x \geq 10$ km, seems to fare worst, indicating that more than 10 km is needed for an IBL to reach equilibrium. It is noteworthy that the σ-values in Tables 3–5 change very little from case to case. Only $\bar{\delta}$ seems to change, the only exception being the last case in which not only $\bar{\delta}$ is increased, but to some extent also σ when forcing h to H for $x \geq 10$ km. Undoubtedly, this is due to the fact that we force an abrupt change into the model response when x passes 10 km.

The seasonal variation of $\bar{\delta}$ is a common characteristic of the three tables. The magnitude of the variation is seen to be characteristic for each mast and quite independent of the different model characteristics and parameter values tested in the various tables.

Part of this variability is probably due to seasonal variability in the larger-scale roughness, which is not taken into account in the model computations and therefore will show up in $\bar{\delta}$. It appears from the tables that the seasonal variability of $\bar{\delta}$ is most pronounced for mast 4. In Appendix A it is shown that mast 4 also is the mast for which we were forced to make the most extensive use of terrain-based assessment of the large-scale roughness. For this mast it is seen from the tables that $\bar{\delta}_{winter} > \bar{\delta}$ for the other seasons. Equation (15) suggests that this might be interpreted as if the large-scale roughness for mast 4 is smaller during winter than during the rest of the year. This simply means that the large-scale roughness, as encountered here, to some extent exhibits a seasonal variation as is found in the roughness for the fields close to the masts. However, the picture is not really clear as the table also show that the seasonal variation of $\bar{\delta}$ is opposite for masts 2 and 3, although much weaker.

The variation found in $\bar{\delta}$ can be related to the variation of z_0. For simplification we shall use the surface layer model only, neglecting the profile kinks. Also, we limit the description to two roughnesses only, z_{01} pertaining to water and z_{02} describing the land roughness.

The modelled ratio between upstream and downstream velocity is found from Section 4

$$\frac{u_2(z)}{u_1(z)} = \frac{\ln \frac{h}{z_{01}}}{\ln \frac{h}{z_{02}}} \cdot \frac{\ln \frac{z}{z_{02}}}{\ln \frac{z}{z_{01}}} \tag{16}$$

Based on the Eqs. (15) and (16) we can find the changes in δ related to changes in z_{01} and z_{02}

$$d\delta = a\frac{dz_{02}}{z_{02}} - b\frac{dz_{01}}{z_{01}} \tag{17}$$

with

$$a = \frac{100}{R_s}\ \frac{u_2}{u_1}\ \frac{\ln\frac{h}{z}}{\ln\frac{h}{z_{02}}\ln\frac{z}{z_{02}}}$$

$$b = \frac{100}{R_s}\ \frac{u_2}{u_1}\ \frac{\ln\frac{h}{z}}{\ln\frac{h}{z_{01}}\ln\frac{z}{z_{01}}}$$

where R_s is the experimentally determined ratio between u_2 and u_1, compare Eq. (15).

With average land fetches of the order of 45, 7 and 2 km for masts 4, 3, and 2, respectively, and with $z_{02} \simeq 20$ cm and $z_{01} \simeq 0.1$ mm, the estimates of the a's and b's are summarized in Table 6 for the different masts.

From Tables 3, 4, or 5 is seen that for mast 4 the winter δ-value is about 8% larger than for the rest of the year. Since most of the roughness between mast 4 and the water is large-scale roughnesses estimated from Table A5 (see Table A4), this means through Eq. (16) that the estimated large-scale roughness is about 80% too high during the winter season. Correspondingly it is seen that the winter roughnesses used for mast 2 and mast 3 are about 30% too small if the winter $\bar{\delta}$-value should be of the same magnitude as for the other seasons.

In Fig. 8 we present the influence of the estimated upstream water roughness by plotting the yearly average values of $\bar{\delta}$ at the three masts for different values of Charnock's constant c. Note that the relative change in water roughness equals the relative change in c.

The influence of Charnock's constant c is shown, using both the extended BL and the SL-model. From the figure is seen that for all three masts the data model comparison is internally consistent in showing that $\bar{\delta} \sim 0$ for $c = 3.0 \times 10^{-2}$ as previously noted. For the SL-model the δ-values at mast 4 look slightly less consistent with those for the two other masts than for the BL-model. However, from Eq. (17) and Table 6 is seen that a 15%

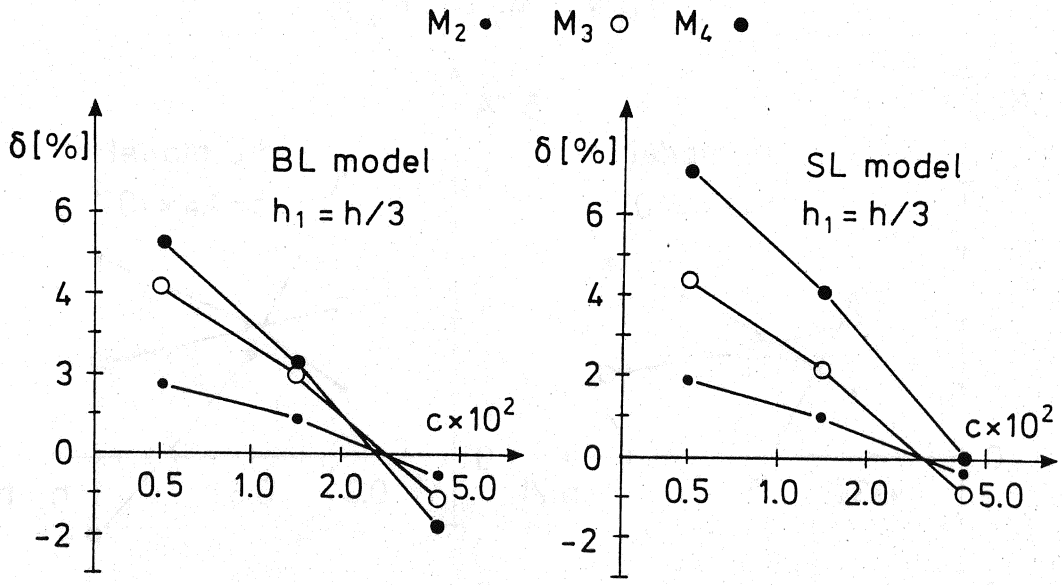

Figure 8: The variation with Charnock's constant, c, of the yearly mean values of $\bar{\delta}$ (see Eq. (15)) for the different masts based on both the full boundary layer model (BL) and the surface layer model (Eq. (9)), denoted SL.

Table 6: Estimates of the sensitivity factors a and b in Eq. (17) for mast 2, 3, and 4.

Mast	a	b
2	5.3	1.02
3	7.6	1.5
4	9.8	2.2

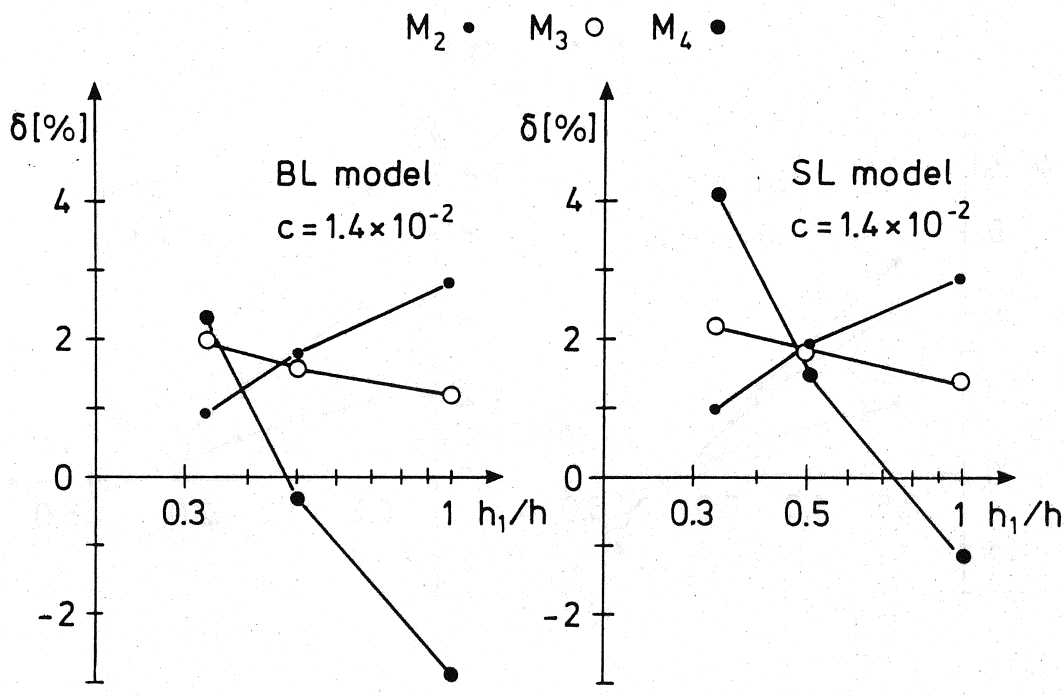

Figure 9: The variation of the yearly mean value of $\bar{\delta}$ (see Eq. (15)) versus the height ratio h_1/h (compare Fig. 7) for the different masts and based on both the full boundary layer model (BL) and the surface layer model (SL). $c = 1.4 \cdot 10^{-2}$.

reduction of large-scale roughness, to which mast 4 is more sensitive that the two other masts, would reverse the picture.

The figure also illustrates that the sensitivity of $\bar{\delta}$ to changes in Charnock's constant increases with distance to the shore line as predicted by Eq. (17) and Table 6.

In Fig. 9 is illustrated the influence of $\bar{\delta}$ of using different values of h_1/h. The difference between the δ's at the three masts increases for $h_1/h > 0.5$. Equation (17) and Table 4 show that this effect cannot be repaired by changing Charnock's constant. Hence, we conclude that the kinked profile with $h_1/h \simeq 0.3$ does indeed improve the performance of the models. This latter point is illustraed in Fig. 10 which corresponds to Fig. 9, but with Charnock's constant $c = 3.0 \times 10^{-2}$.

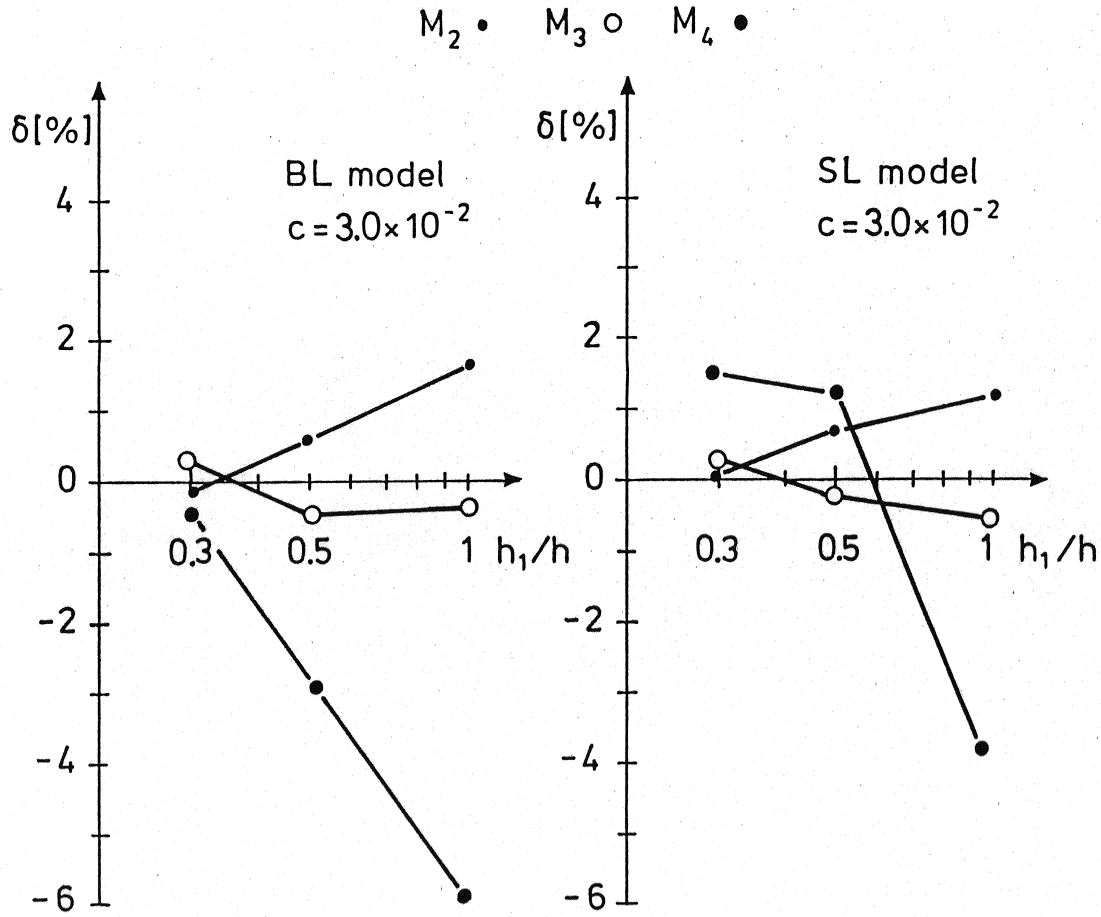

Figure 10: The variation of the yearly mean value of $\bar{\delta}$ (see Eq. (15)) versus the height ratio h_1/h (compare Fig. 9) for the different masts and based on both the full boundary layer model (BL) and the surface layer model (SL). $c = 3.0 \cdot 10^{-2}$.

7 Conclusion and discussion

We have studied the flow response to roughness changes when air flows inland from a coast. We have discussed both data and simple models and used comparisons between the two to evaluate parameter choices for the models as well as the sensitivity of model outputs to parameter choices.

It was found that the uncertainty of the roughness and fetch values not directly measured, made any certain evaluation of model performances impossible. With this uncertainty in mind, we conclude that comparison between models and data indicates that both the simple surface layer model and the extended form discussed here perform reasonably and equally well. This is true despite the essential incorrectness of both models for large fetches where they either do not approach a new equilibrium situation or approach it too slowly. With this in mind we tried to force the models to approach equilibrium at a distance of 10 km. However, the model thus forced, performed worse than the non-forced version.

The comparison between models and data indicates that the upstream water roughness should be somewhat larger than indicated by open-ocean data. However, the optimum value found by us fits quite well data from measurements in the nearby German Bight by Geenaert et al. (1987), who argue for physical reasons as well that the water closer to the shore should be rougher than the open ocean.

We have illustrated the seasonal variation of the surface roughness over land. From the measurements we conclude that the land has an overall higher roughness during summer than winter. For fields close to the measuring masts we are able to follow the seasonal variation of roughness. By means of photographs we were able to see how this roughness follows the growth cycle of the crop, and we found that in the growing season the profile roughness closely matches well-known formulas that related z_0 to the height of vegetation (see e.g. Thom, 1971 and Brutsaert, 1975). To make estimates of the larger-scale roughness we were forced to fall back on the standard rule-of-thumb relations between types of terrain and roughness (see Table A5). This criterion yields no information on a seasonal variation of the roughness. However, by comparing the measured and modelled reductions of wind speed we found that the larger-scale roughness varies also with season, being smallest during winter.

Acknowledgements

The authors acknowledge useful discussions with N.O. Jensen, E.L. Petersen and T. Mikkelsen. We also wish to acknowledge that virtually each and every member of the Department of Meteorology and Wind Energy at Risø National Laboratory has been involved in running the JYLEX-experiment. Especially we wish to acknowledge G. Dalsgaard, G. Jensen and M. Frederiksen for their work on establishing the measuring stations, running the data sampling system, and compiling the auxiliary information, respectively.

The experiment and analysis were supported by grants from the Danish Ministry of Energy (EFP–22564–81 and EFP–22528–412).

References

Bradley, E.F. (1968). A micrometeorological study of velocity profiles and surface drag in the region modified by a change in surface roughness. *Quart. J.R. Met. Soc.*, **94**, 361-379.

Brutseart, W. (1975). Comments on surface roughness parameters and the height of dense vegetation. *J. Met. Soc. Japan*, **53**, 96-97.

Businger, J.A. (1972). The atmospheric boundary layer. In: Remote Sensing of the Troposphere. Ed. V.E. Derr (US Govt. Printing Office, Wash. DC COM/72/51061) 6/1 - 6/51.

ESDU 72026 (1972). Characteristics of wind speed in the lowest layers of the atmosphere near the ground: strong winds. Eng. Sci. Data Unit Ltd., 251 Regent St., London W1R 7AD.

Geernaert, G.L., S.E. Larsen and F. Hansen (1987). Measurements of the wind stress, heat flux, and turbulence intensity during storm conditions over the North Sea. *J. Geophys. Res.*, **92**, 13127-13139.

Hedegaard, K. and S.E. Larsen (1982). Wind speed and directional changes due to terrain effects revealed by climatological data from two sites in Jutland. Risø–R–434.

Jensen, N.O., E.L. Petersen and I. Troen (1984). Extrapolation of mean wind statistics with special regard to wind energy application. WCP-86. WMO.

Jensen, N.O. and E.W. Peterson (1977). Wind flow near the surface over nonuniform terrain. Report of progress for the year 1976 (progress report for US Army Grant, available at Risø National Laboratory).

Jensen, N.O. (1978): Change of surface roughness and the planetary boundary layer. *Quart. J.R. Met. Soc.*. **104**, 351-356.

Larsen, S.E., K. Hedegaard and I. Troen (1982): The change of terrain roughness problems extended to mesoscale fetches. In: Proc. First International Conference on Meteorology and Air/Sea Interaction (Amer. Meteor. Soc., Boston, USA and KNMI, the Netherlands), 8-13.

Larsen, S.E. and N.O. Jensen (1983): Summary and interpretation of some Danish climate statistics. Risø–R–399.

Mahrt, L. and S.E. Larsen (1982): Small scale drainage front. *Tellus*, **34**, 579-587.

Miyake, M. (1965). Transformation of the atmospheric boundary layer over inhomogeneous surfaces. Scientific report, University of Washington, Seattle.

Panofsky, H.A. (1973): Tower climatology. In: Workshop on Micrometeorology. Ed. D.A. Haugen (Amer. Meteorol. Soc., Boston, USA), 177-216.

Petersen, E.L. and I. Troen (1986): The European Wind Atlas. In: Proc. of the EWEC'86 Conference, Rome, Italy, 7-9 October, 1986. 55-65.

Peterson, E.W. (1972): Relative importance of terms in the turbulent energy and momentum equations as applied to the problem of a surface roughness change. *J. Atmos. Sci.*, **29**, 1470-1476.

Peterson, E.W., N.O. Jensen and J. Højstrup (1979). Observations of downwind development of wind speed and variance profiles at Bognæs and comparison with theory. *Quart. J. Roy. Met. Soc.*, **105**, 521-529.

Rao, K.S., J.C. Wyngaard and D.R. Coté 1974): The structure of the two-dimensional internal boundary layer over a sudden change of surface roughness. *J. Atmos. Sci.*, **26**, 432-440.

Taylor, P.A. (1969). The planetary boundary layer above a change in surface roughness. *J. Atmos. Sci.*, **26**, 432-440.

Tennekes, H. (1973): Similarity laws and scale relations in planetary boundary layers. In: Workshop on Micrometeorology. Ed. D.A. Haugen, Amer. Meteor. Soc., Boston, USA, 177-216.

Thom, A.S. (1971): Momentum absorption by vegetation. *Quart. J. R. Met. Soc.*, **97**, 414-428.

A Roughness and fetch conditions for the four masts

The determination of the relevant fetches for each mast has been a hybrid enterprise involving maps, inspection trips, photographs and measured velocity profiles.

As the situation becomes more and more ambiguous as we move inland, we shall start discussing mast 1. This mast looks over the water of Ringkøbing Fjord which is separated from the North Sea about 10 km to the west by a narrow ($\sim$ 400 m) isthmus (see Fig. 1). In the following we shall neglect this isthmus in general and consider the fjord and North Sea to be one uniform water surface with a roughness z_{ow}, given by Eq. (1).

Between the water and mast 1 is a narrow belt of rush which after harvesting in late winter/early spring grows until slightly less than 2 m by the end of the summer and remains so until next harvesting. The roughness of this rush was determined by the data in sector 9 which was the only sector with sufficient rush fetch to allow the profile method to be used for determining the displacement length d and roughness z_0. The roughness found was then taken as the proper value for the other sectors as well. The d and z_0 values found were in accordance with the generally accepted relations between height of vegetation, d and z_0 for this kind of vegetation (see e.g. Thom, 1971). The rush fetch was evaluated from maps and inspections to the site. The resulting list of fetches and roughnesses are as shown in Table A1. It is seen that the influence of the rush surface will not reach the 31-m level, which is the level used to infer the upstream over-water condition, except for perhaps sector 9. Therefore, this sector was dropped in the study involving the comparison between data and the different models.

Mast 2 is placed on the eastern side of a field bordering the rush roughly 800 m to the west of the mast. For most sections, therefore, the roughness and fetch conditions for mast 2 are easy to determine: the field roughness is found by the profile method described above while the roughness of the rush was found in connection with mast 1. For mast 2 we are accordingly able to describe most roughness values of interest as a function of season. Only for sectors 8 and 9 do we have to describe the roughness of mixed areas (fields, hedges, trees, and houses). For these sectors, therefore, we used only one roughness for the entire year for the large-scale fetches.

The roughness and fetch description for mast 2 is presented in Table A2.

Table A3 contains the roughness and fetch descriptions used for mast 3. The near-field roughness is again determined from the profiles, and the seasonal variation is seen to reflect much the same crop pattern as for mast 2. For the large-scale roughness areas we used the z_0-values from Table A5 after ESDU (1972), (Jensen et al., 1984).

In connection with this mast, it was found that sector 1 followed the south coast of the fjord in such a way that the sectors for these fetches are half water and mud and rush fields and half land (see also Fig. 3). As we were unable to give a good roughness description for this combination we have neglected this sector in the data compilation.

Finally, we show the fetch and roughness conditions at mast 4 in Table A4. This table reflects the same principles as those of Tables A1 and A2. For the near-field roughness the seasonal variation is different from the patterns at the other masts. This reflects differences in vegetation. At mast 4 the field was laid down to grass.

Table A1: Roughness lengths and fetches of the flow directions considered for mast 1. z_{0w} is the upstream water roughness computed from Eq. (1).

Sector	Direction [°]	z_{01} [cm]	x_1 [m]	z_{02} [cm]	Season
1	230	10.0	75	z_{0w}	winter
		3.0			spring
		7.0			summer
		10.0			fall
2	240	10.0	75	z_{0w}	winter
		3.0			spring
		7.0			summer
		10.0			fall
3	250	10.0	75	z_{0w}	winter
		3.0			spring
		7.0			summer
		10.0			fall
4	260	10.0	75	z_{0w}	winter
		3.0			spring
		7.0			summer
		10.0			fall
5	270	10.0	100	z_{0w}	winter
		3.0			spring
		7.0			summer
		10.0			fall
6	280	10.0	110	z_{0w}	winter
		3.0			spring
		7.0			summer
		10.0			fall
7	290	10.0	110	z_{0w}	winter
		3.0			spring
		7.0			summer
		10.0			fall
8	300	10.0	150	z_{0w}	winter
		3.0			spring
		7.0			summer
		10.0			fall
9	310	10.0	1150	z_{0w}	winter
		3.0			spring
		7.0			summer
		10.0			fall

Table A2: Roughness lengths and fetches of the flow directions considered for mast 2. z_{0w} is the upstream water roughness computed from Eq. (1).

Sector	Direction [°]	z_{01} [cm]	x_1 [m]	z_{02} [cm]	x_2 [m]	z_{03} [cm]	Season
1	230	0.5 0.3 5.0 1.9	650	10.0 3.0 7.0 10.0	975	z_{0w}	winter spring summer fall
2	240	0.5 0.4 5.0 2.2	575	10.0 3.0 7.0 10.0	750	z_{0w}	winter spring summer fall
3	250	0.5 1.0 1.0 2.6	600	10.0 3.0 7.0 10.0	750	z_{0w}	winter spring summer fall
4	260	0.8 1.6 5.0 2.5	600	10.0 3.0 7.0 10.0	775	z_{0w}	winter spring summer fall
5	270	0.9 1.5 5.0 2.3	825	10.0 3.0 7.0 10.0	1200	z_{0w}	winter spring summer fall
6	280	0.9 1.3 5.0 2.3	1000	10.0 3.0 7.0 10.0	1425	z_{0w}	winter spring summer fall
7	290	0.8 1.0 5.0 2.0	900	10.0 3.0 7.0 10.0	1525	z_{0w}	winter spring summer fall
8	300	0.7 0.8 5.0 1.8	1125	10.0	2250	z_{0w}	winter spring summer fall
9	310	0.5 0.6 5.0 1.5	1250	20.0	3100	z_{0w}	winter spring summer fall

Table A3: Roughness lengths and fetches of the flow directions considered for mast 3. z_{0w} is the upstream water roughness computed from Eq. (1).

Sector	Direction [°]	z_{01} [cm]	x_1 [km]	z_{02} [cm]	x_2 [km]	z_{03} [cm]	Season
1	230	0.4 0.5 3.8 1.4	5.75	z_{0w}			winter spring summer fall
2	240	0.5 0.2 4.0 1.2	5.3	z_{0w}			winter spring summer fall
3	250	0.5 0.5 1.8 1.0	4.7	z_{0w}			winter spring summer fall
4	260	0.6 0.9 3.2 2.0	2.5	10	4.3	z_{0w}	winter spring summer fall
5	270	0.4 0.7 8.0 2.0	2.63	20	4.4	z_{0w}	winter spring summer fall
6	280	0.4 0.5 6.0 1.7	2.75	10	4.55	z_{0w}	winter spring summer fall
7	290	0.2 0.3 6.0 1.3	0.9	20	5.43	z_{0w}	winter spring summer fall
8	300	0.2 0.3 5.0 1.8	1.0	20	7.23	z_{0w}	winter spring summer fall
9	310	0.3 0.5 4.4 0.6	0.9	20	10.73	z_{0w}	winter spring summer fall

Table A4: Roughness lengths and fetches at mast 4. z_{0w} is the upstream water roughness computed from Eq. (1).

Sector	Dir. [°]	z_{01} [cm]	x_1 [km]	z_{02} [cm]	x_2 [km]	z_{03} [cm]	x_3 [km]	z_{04} [cm]	x_4 [km]	z_{05} [cm]	x_5 [km]	z_{06} [cm]	Season
1	230	0.7 0.5 0.9 0.8	0.6	20.0	9.3	2.0	13.5	20.0	56.25	z_{0w}			winter spring summer fall
2	2 40	0.4 0.5 0.8 1.2	0.9	30.0	9.5	2.0	14.0	30.0	48.0	z_{0w}			winter spring summer fall
3	250	0.3 0.4 1.0 1.6	1.0	20.0	22.3	10.0	31.5	0.001	37.2	20.0	48.0	z_{0w}	winter spring summer fall
4	260	0.3 0.2 0.6 1.0	1.0	30.0	23.2	10.0	28.0	z_{0w}					winter spring summer fall
5	270	0.9 0.3 2.6 1.6	0.8	30.0	26.0	10.0	30.7	z_{0w}					winter spring summer fall
6	280	0.9 0.7 1.8 1.7	0.6	30.0	28.0	10.0	32.0	z_{0w}					winter spring summer fall
7	290	0.9 0.9 2.1 1.3	0.5	30.0	37.5	10.0	46.2	z_{0w}					winter spring summer fall
8	300	1.0 1.2 1.6 1.3	0.5	30.0	40.0	5.0	48.4	z_{0w}					winter spring summer fall
9	310	1.1 1.0 1.6 1.5	0.5	30.0	56.25	z_{0w}							winter spring summer fall

Table A5:

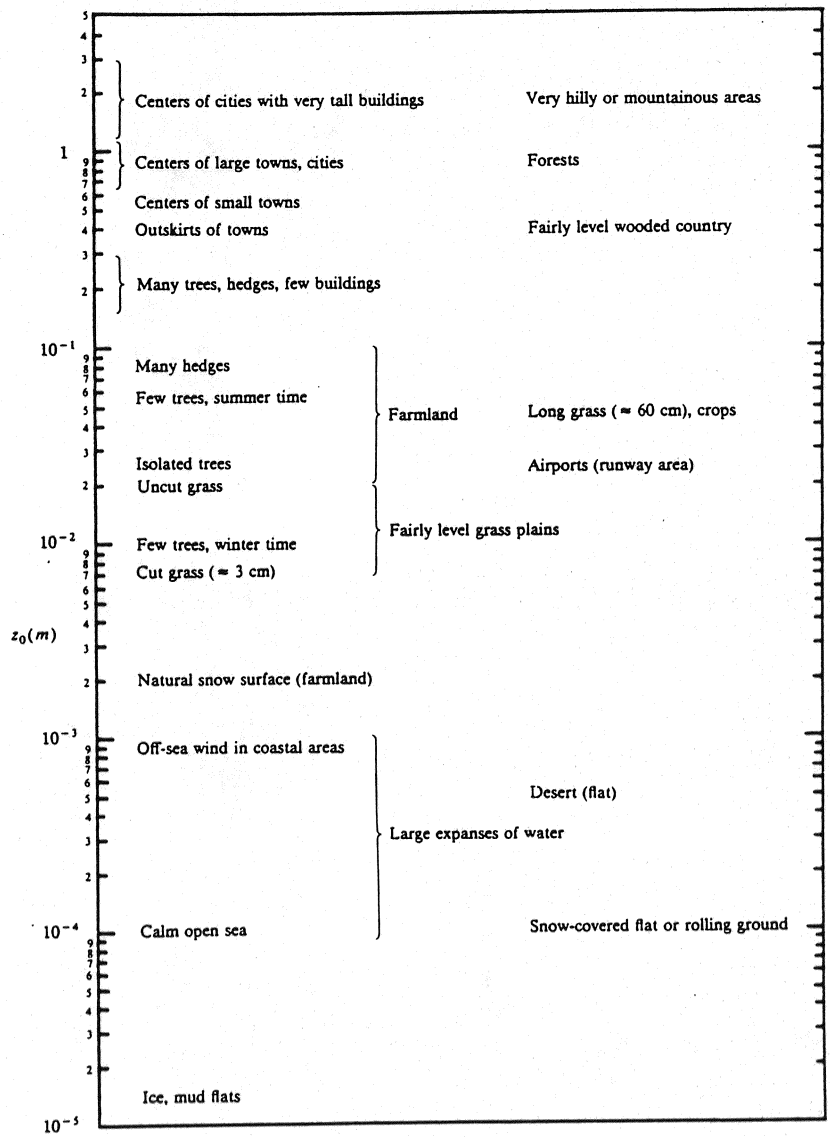
Centers of cities with very tall buildings
Very hilly or mountainous areas
Centers of large towns, cities
Forests
Centers of small towns
Outskirts of towns
Fairly level wooded country
Many trees, hedges, few buildings
Many hedges
Few trees, summer time
Farmland
Long grass (≈ 60 cm), crops
Isolated trees
Airports (runway area)
Uncut grass
Fairly level grass plains
Few trees, winter time
Cut grass (≈ 3 cm)
$z_0(m)$
Natural snow surface (farmland)
Off-sea wind in coastal areas
Desert (flat)
Large expanses of water
Calm open sea
Snow-covered flat or rolling ground
Ice, mud flats

Risø National Laboratory **Risø–M–2749**

Title and author(s)

Roughness change effects of small and large fetches

Anna Maria Sempreviva
S.E. Larsen
N.G. Mortensen
and Ib Troen

Date October 1988

Department or group
Meteorology
and Wind Energy

Groups own registration no.

Project/contract no.
EM-22564-81,
EM-22528-412

Pages 49 Tables 11 Illustrations 10 References 21

ISBN 87–550–1467–4

Abstract (max. 2000 characters)

Measurements were obtained during a two-year period along four meteorological masts placed from the coastline to 30 km inland at the North Sea coast of Jutland in Denmark (JYLEX).
From these data the near neutral cases were selected. The data are organized to show the reduction of wind speed as a function of inland fetch. The results are stratified according to season and are compared with a simple model description of the response of the neutral boundary layer to step changes in surface roughness.

Descriptors – EDB

BOUNDARY LAYERS; COASTAL REGIONS; ROUGHNESS; SEASONAL VARIATIONS; TOPOGRAPHY; VELOCITY; WIND

Available on request from Risø Library, Risø National Laboratory (Risø Bibliotek, Forskningscenter Risø)
P.O. Box 49, DK–4000 Roskilde, Denmark. Telephone: 02 37 12 12, ext. 2262. Telex: 43116, Telefax: 02 36 06 09